Letter

Zero-energy corner states in a non-Hermitian quadrupole insulator

Yang Yu,[1] Minwoo Jung,[2] and Gennady Shvets[1,*]
[1]*School of Applied and Engineering Physics, Cornell University, Ithaca, New York 14853, USA*
[2]*Department of Physics, Cornell University, Ithaca, New York 14853, USA*

(Received 11 March 2020; accepted 10 December 2020; published 5 January 2021)

We point out that in non-Hermitian systems, Jordan decomposition should replace eigendecomposition so that all "good approximate eigenstates" of the system are identified. These states can be resonantly excited. As a concrete example, we study the location and field distribution of zero-energy corner states in a non-Hermitian quadrupole insulator (QI) and split the parameter space into three distinct regimes according to properties of the corner states: near-Hermitian QI, intermediate phase, and trivial insulator. In the newly discovered intermediate phase, the Hamiltonian becomes defective, and the counterintuitive and delicate response of the system to external drives can be perfectly explained by the Jordan decomposition.

DOI: 10.1103/PhysRevB.103.L041102

Introduction. Higher-order topological insulators (HOTIs) are characterized by exotic topological signatures with dimensionality that is lower by at least two than that of the protecting bulk. One such signature is fractionally quantized corner charges in two-dimensional (2D) crystals with C_n symmetry [1]. In the presence of an additional chiral (sublattice) symmetry, $e/2$ corner charges become associated with mid-gap ("zero-energy") corner-localized states [1]. Similar fractionalized vortex states can also exist *inside* a 2D lattice with appropriate order parameter twists [2]. While the fractional nature of the topological charge is of particular significance for fermionic systems, the localized nature and robust spectral pinning of such corner/vortex states is of great practical importance for bosonic (e.g., acoustic, photonic, and radio-frequency) lattices [3–6]. Among many types of HOTIs supporting zero-energy corner states, the quadrupole insulator (QI) is a particularly interesting one because its lowest nonvanishing bulk polarization moment is quadrupolar [7,8], i.e., its dipole polarization moment strictly vanishes. QI is the first type of HOTI to be theoretically predicted [7] and experimentally implemented [3,4].

Non-Hermitian physics also attracted considerable interest in recent years because of its relevance to nonequilibrium (e.g., undergoing photoionization) systems [9,10]. Some of its notable phenomena include "exceptional points" (EPs) [11–13] and real-valued spectra despite non-Hermiticity. At the EP, both the complex-valued eigenvalues of two bands as well as their corresponding eigenvectors coalesce [14,15]. In other words, the matrix corresponding to the Hamiltonian at the EP becomes *defective* [16,17]. The completely real spectrum of some non-Hermitian systems can be related to parity-time (PT) symmetry [18–20] or pseudo-Hermiticity [21], though in general it is hard to assert a real spectrum without directly calculating the eigenvalues.

Extending the rich and rapidly growing field of topological physics to non-Hermitian systems has been of great interest [22–24] because of their relevance to nonequilibrium topological systems [25,26]. However, most literature just simply uses eigendecomposition, but it is known in numerical computation that eigendecomposition is only suited for Hermitian matrices [16]. This leads to not correctly identifying all "good approximate eigenstates" of the system that can be resonantly excited. In this Letter we point out it is crucial to use Jordan decomposition (or in numerical studies, Schur decomposition [16]) in non-Hermtian systems. While this claim is quite general, a non-Hermitian version of a QI model proposed in Ref. [7] serves as a nice lattice model for demonstration. We focus on the behaviors of its zero-energy corner states, and show that Jordan decomposition can beautifully explain the delicate response of the system to external drives.

Tight-binding model. The non-Hermitian QI model studied in this Letter is schematically shown in Fig. 1(a), where the intra/intercell hopping amplitudes $t \pm \gamma$ and λ are all taken to be real. It is a natural non-Hermitian generalization of the QI model described in Ref. [7], with the intracell hopping strength becoming asymmetric, characterized by a finite γ, while maintaining the sublattice symmetry $\Sigma H \Sigma^{-1} = -H$. Here the symmetry operator $\Sigma = P_1 - P_2 - P_3 + P_4$, where $P_j = \sum_{x,y} |x, y, j\rangle\langle x, y, j|$ are the sublattice projection operators, and $|x, y, j\rangle$ are the tight-binding states, where x and y are integer-valued coordinates of the unit cells as defined in Fig. 1(a), and $j = 1, \ldots, 4$ denote four sublattice sites of each unit cell. This model can also be viewed as a two-dimensional (2D) generalization of the non-Hermitian Su-Schrieffer-Heeger (SSH) model [23,27,28].

Non-Bloch bulk continuum. As was pointed in the context of the non-Hermitian SSH system [23], the open-boundary spectrum can significantly differ from that of the periodic-boundary system described by the Bloch Hamiltonian $H(\vec{k})$. That is because the usual Bloch phase-shift factor e^{ik} for bulk eigenstates (i.e., eigenstates in the continuum spectrum) of an open-boundary system needs to be modified to $\beta \equiv \beta_0 e^{ik}$, where β_0 can be nonunity (i.e., the wave vector acquires an imaginary part: $k \to k - i \ln \beta_0$). This extra *bulk localization factor* β_0 must be taken into account

*gshvets@cornell.edu

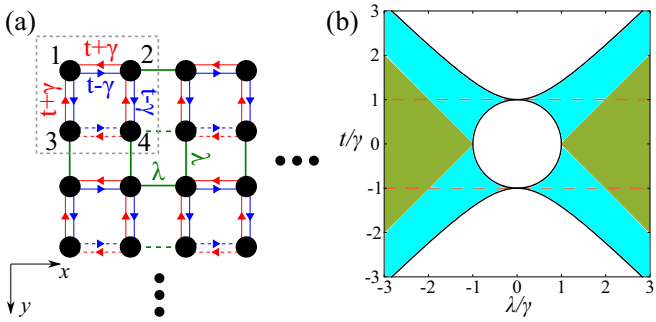

FIG. 1. (a) Tight-binding model of a non-Hermitian QI on a square lattice. Gray dashed line: Boundary of unit cell with four (sublattice) sites (numbered 1 to 4). Red and blue lines with arrows: Asymmetric intracell hopping amplitudes $\pm t \pm \gamma$. Green lines: Symmetric intercell hopping amplitudes $\pm\lambda$. Dashed lines: Negative hopping terms. All four sublattices have the same on-site potentials (set to $\epsilon_j \equiv 0$). (b) The phase diagram of a large non-Hermitian QI with open-boundary condition. Green region ($|\lambda| > |t| + |\gamma|$): Near-Hermitian regime with four zero-energy corner states, each localized at a separate corner. Cyan region ($\sqrt{|t^2 - \gamma^2|} < |\lambda| < |t| + |\gamma|$): Intermediate regime with two zero-energy corner states at the top-left corner. White region ($|\lambda| < \sqrt{|t^2 - \gamma^2|}$): No corner states. Band gap vanishes along solid black lines. The spectrum is complex valued between the two dashed orange lines, real valued elsewhere.

when calculating the spectrum of the open-boundary system. The same argument applies to our 2D non-Hermitian QI system, where $\vec{k} \equiv (k_x, k_y) \to (k_x - i \ln \beta_0, k_y - i \ln \beta_0)$, and $\beta_0 = \sqrt{|(t-\gamma)/(t+\gamma)|}$ [24]. With this substitution the corrected Bloch Hamiltonian shows agreement [29] with numerical simulations of an open-boundary system, that a finite bulk band gap exists for all values of the hopping amplitudes except at $t^2 = \gamma^2 \pm \lambda^2$. The zero-gap condition is represented in Fig. 1(b) by the solid black lines.

Another important consequence of this extra factor β_0 is that the bulk spectrum is real valued for $|t| > |\gamma|$. While there are also edge and corner states, our numerical results show that the entire spectrum is real for arrays of any size whenever $|t| > |\gamma|$. This fact can be related to the pseudo-Hermiticity of the Hamiltonian [24].

Zero-energy corner states. Having established the bulk properties of non-Hermitian QIs, we now proceed with investigating the existence conditions and spatial properties of zero-energy corner states supported by a large ($N \times N$ array, $N \gg 1$) non-Hermitian QI with open-boundary conditions. In what follows, we focus on the systems with entirely real-valued spectrum: $t > \gamma > 0$ and $\lambda > 0$. When the intercell hopping strength dominates over the intracell one, i.e., $\lambda > t + \gamma$, it can be shown that the four corner states identified in Hermitian QIs [7,30] still persist in the thermodynamic limit $N \gg 1$ (where the coupling between different corners of the domain is negligible), albeit with modified field distributions [29]:

$$|\psi_1\rangle = \sum_{x,y} \left(-\frac{t-\gamma}{\lambda}\right)^{x+y} |x, y, 1\rangle, \tag{1a}$$

$$|\psi_2\rangle = \sum_{x,y} \left(-\frac{t+\gamma}{\lambda}\right)^{-x} \left(-\frac{t-\gamma}{\lambda}\right)^{y} |x, y, 2\rangle, \tag{1b}$$

$$|\psi_3\rangle = \sum_{x,y} \left(-\frac{t-\gamma}{\lambda}\right)^{x} \left(-\frac{t+\gamma}{\lambda}\right)^{-y} |x, y, 3\rangle, \tag{1c}$$

$$|\psi_4\rangle = \sum_{x,y} \left(-\frac{t+\gamma}{\lambda}\right)^{-x-y} |x, y, 4\rangle. \tag{1d}$$

Just as in the case of a Hermitian QI, each corner state is localized at one corner of the array, and has support on only one sublattice. The asymmetric intracell coupling is the reason for the different states to have different spatial localization lengths, and for those lengths to be different in the x and y directions. Therefore, we refer to this parameter regime as "near-Hermitian." Figure 2 presents the field distributions of the four corner states [see Fig. S1(a) for the full spectrum].

An earlier work has incorrectly concluded that all four corner eigenstates are localized in the upper-left corner [24] as shown in Fig. 2(a). The reason for this numerical artifact is the finite (albeit exponentially small in the system size) coupling between different corner states. This coupling is asymmetric because of the non-Hermiticity of the Hamiltonian, resulting in one of the corner states dominating the others in the coupled eigenstates. However, these coupling coefficients should not be compared with each other. Rather, it is only physically justifiable to compare them with a characteristic energy width ΔE of the system, e.g., the loss rate of a realistic system, or the inverse of the observation timescale, or the energy splitting of the two corner states due to system imperfections. If all the coupling coefficients are much smaller than ΔE, which will be true for a large enough N, then Eq. (1) are the good approximate eigenstates of the system. In numerical studies this issue can be overcome by using Schur decomposition, as in Fig. 2. Similar misconceptions have appeared in, for example, Ref. [31], which again comes from the improper use of eigendecomposition in non-Hermitian systems.

As we enter the *intermediate* regime $\sqrt{t^2 - \gamma^2} < \lambda < t + \gamma$ range, see Fig. 1(b), only the first of the above four corner states survives, see Fig. 3(a). Additionally, a new corner state—also localized at the top-left corner, but having support on two (2 and 3) sublattices—emerges. It has the following field distribution [29]:

$$|\phi\rangle = \sum_{x,y} (r_1^x - r_2^x) r_1^y (|x, y, 2\rangle - |y, x, 3\rangle), \tag{2}$$

where $r_1 = -(t-\gamma)/\lambda$, $r_2 = -\lambda/(t+\gamma)$, see Fig. 3(b). Similar corner states have been predicted in a Hermitian model, but there the bulk is gapless [30]. We refer to the surviving ψ_1 as "monosublattice," and the less localized (since $|r_2| > |r_1|$) ϕ as "multisublattice." This contrast of localization length is evident in Fig. 3 [see Fig. S1(b) for the full spectrum]. Both states are corner states since they have a different localization factor than that of bulk states β_0. The change of the location of corner states has been observed in the non-Hermitian SSH model as well [23].

Although the numerical eigenvalue calculation shows zero eigenenergy of multiplicity four, these two corner states are the only two linearly independent eigenstates, which will be shown later. This implies that the Hamiltonian is defective at zero energy—a common feature of non-Hermitian systems [17]. Remarkably, the Hamiltonian is not defective at zero

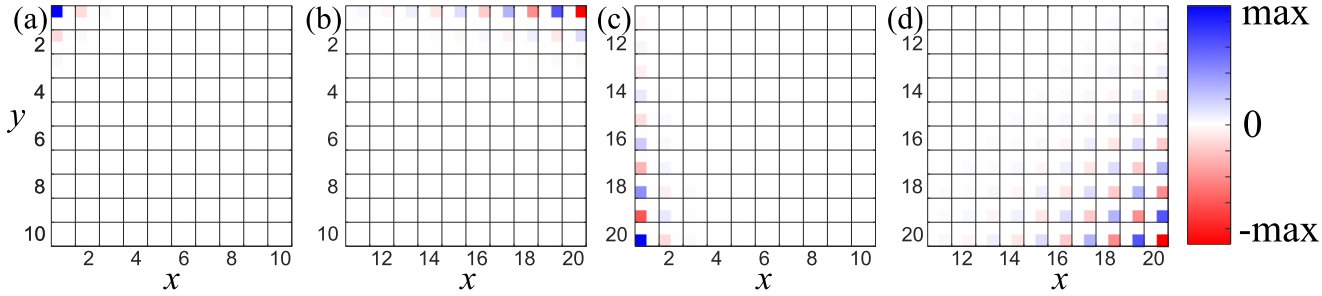

FIG. 2. Field distribution of the four zero-energy (mid-gap) corner states of a large square domain of a non-Hermitian QI in the "near-Hermitian" regime $t = 0.6$, $\gamma = 0.4$, $\lambda = 1.5$, obtained using Schur decomposition. Domain size: 20×20 unit cells.

energy in the near-Hermitian regime. Thus, the transition between these two regimes is not induced via a bulk band gap closure.

When the intercell hopping amplitude is further reduced to $\lambda < \sqrt{t^2 - \gamma^2}$, zero-energy corner states disappear (trivial regime). The three regimes of a square finite-sized non-Hermitian QI with open-boundary conditions are summarized by a phase diagram shown in Fig. 1(b). Only trivial and near-Hermitian regimes have been previously identified [24]. Below we demonstrate that the neglected intermediate regime exhibits highly counterintuitive behaviors such as nonlocal excitation and unidirectional amplification of corner states.

Excitation of corner states. Having classified the number and properties of zero-energy corner states in 2D non-Hermitian QI, we now discuss how to observe them. In bosonic systems a (periodic) drive corresponds to adding a source term ξ to the equation of motion of the system: $id\psi/dt = H\psi + \xi$. Because the spectrum of the system is purely real when $|t| > |\gamma|$, adding an overall small loss to the system ensures that all transients eventually decay. Therefore, only the driven equation $(E - H)\psi = \xi$ needs to be solved, where E is the driving frequency. If H is not defective (E_n's are eigenvalues), one can still obtain an expression similar to the one in the Hermitian case: $(E - H)^{-1} = \sum_n |\eta_n^R\rangle\langle\eta_n^L|/(E - E_n)$, provided that the left and right eigenvectors of H are normalized according to the bi-orthogonality condition: $\langle\eta_m^L|\eta_n^R\rangle = \delta_{mn}$ [32]. When H is defective this expression must be modified.

In the near-Hermitian regime, not surprisingly, the most efficient excitation of a corner state occurs when the source is placed at the same corner and same sublattice [29]. This behavior is expected based on our intuition derived from the property of the eigenstates $\langle x|\eta_n^R\rangle = \langle\eta_n^L|x\rangle^*$ of the fully Hermitian systems [3–6]. The situation changes dramatically in the intermediate regime. The responses of the system introduced in Fig. 3 (see the caption for the lattice parameters) to external sources localized at different sublattice sites are shown in Figs. 4(a)–4(c). For this numerical study we have chosen $E = 0.01i$, a small uniform on-site loss. Surprisingly, our simulations reveal that the response is "nonlocal": placing the source at the bottom-right corner gives the strongest excitation of the top-left corner states. This contradicts our intuition developed by studying Hermitian systems, where one finds it most efficient to place the source in close proximity of the targeted state's maximum. This contradiction is resolved by noting that the left and right eigenstates of a non-Hermitian system can be very different. Moreover, we find that the response is very sensitive to which sublattice the source is on: the monosublattice state is predominantly excited by placing the source on the sublattices 1, 2, or 3. On the other hand, the multisublattice state is predominantly excited when the source is on sublattice 4. Finally, the response in the intermediate regime is much larger compared to that of near-Hermitian regime (at least 4 orders of magnitude: compare Figs. S2 and 4).

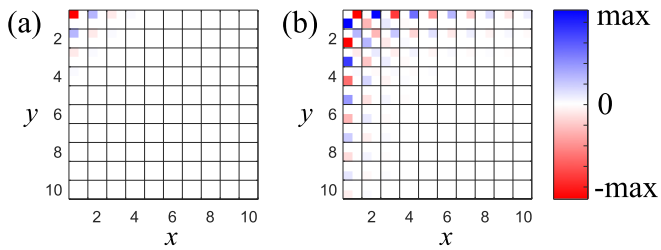

FIG. 3. Corner states of a non-Hermitian QI in the intermediate regime $t = 0.6$, $\gamma = 0.4$, $\lambda = 0.7$. (a) Field distribution of the monosublattice state: similar to Fig. 2(a). (b) The emerging multisublattice state: also localized at the top-left corner, but supported on the sublattices 2 and 3. Domain size: 20×20 unit cells.

Partial Jordan decomposition of Hamilton. As mentioned above, for a non-Hermitian system, the Jordan decomposition is required to explain its spectral properties. We focus on the Jordan blocks for $E = 0$ that are relevant to zero-energy corner states (thus we call it "partial"). In general this task can be performed by the numerical Schur decomposition, while our model is analytically solvable. In this section we use the partial Jordan decomposition to explain why the system has such a delicate and nonlocal response in the intermediate regime. We also prove that there are only two linearly independent corner states in this regime. Numerical results for Fig. 3 show that $E = 0$ is an eigenvalue of H with algebraic multiplicity 4. From the experience of obtaining Eq. (2), it is not too difficult to see that the following four vectors can serve as the four columns of the Jordan basis matrix P corresponding to the $E = 0$ Jordan blocks:

$$|\eta_1^R\rangle = \sum_{x,y} r_1^{x+y} |x, y, 1\rangle,$$

$$|\eta_2^R\rangle = \sum_{x,y} \left(r_1^x - r_2^x\right) r_1^y (|x, y, 2\rangle + |y, x, 3\rangle),$$

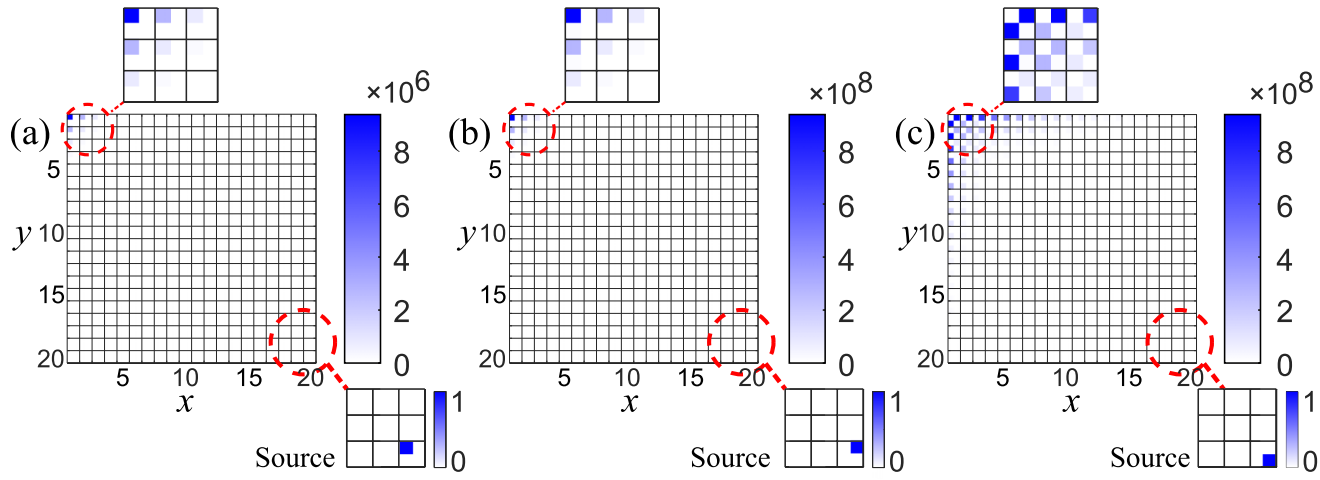

FIG. 4. The response of a non-Hermitian QI in the intermediate regime to external sources placed at different sublattice sites in the lower-right corner of the domain. The source sublattice sites are 1 (left), 2 (middle), and 4 (right). Color: Magnitude of the complex field ψ. Monosublattice (left and middle) and multisublattice (right) corner states are predominantly excited (cf. Fig. 3). Source frequency: $E = 0.01i$, a small uniform on-site loss. Other lattice parameters (domain size and hopping amplitudes) of the tight-binding model: same as in Fig. 3.

$$|\eta_3^R\rangle = \sum_{x,y} \left(r_1^x - r_2^x\right) r_1^y (|x, y, 2\rangle - |y, x, 3\rangle),$$
$$|\eta_4^R\rangle = \sum_{x,y} \left(r_1^x - r_2^x\right)\left(r_1^y - r_2^y\right)|x, y, 4\rangle, \tag{3}$$

and the Jordan blocks for $E = 0$ are

$$J_0 = \begin{pmatrix} 0 & 2\kappa & 0 & 0 \\ 0 & 0 & 0 & 0 \\ 0 & 0 & 0 & \kappa \\ 0 & 0 & 0 & 0 \end{pmatrix}, \tag{4}$$

where $\kappa = t + \gamma - \lambda^2/(t - \gamma)$. We observe from J_0 that the geometric multiplicity of the $E = 0$ eigenvalue is 2, indicating that the $E = 0$ subspace is defective. Note that $|\eta_1^R\rangle$ is the monosublattice state given by Eq. (1a), and $|\eta_3^R\rangle$ is the multisublattice state given by Eq. (2).

Next, the corresponding four rows of P^{-1} must be determined. This can be done by repeating the above analysis for H^T. It turns out they are localized at the bottom-right corner:

$$\langle\eta_1^L| = A_1 \sum_{x,y} \left(r_1^{\bar{x}} - r_2^{\bar{x}}\right)\left(r_1^{\bar{y}} - r_2^{\bar{y}}\right)\langle x, y, 1|,$$
$$\langle\eta_2^L| = A_2 \sum_{x,y} r_1^{\bar{x}}\left(r_1^{\bar{y}} - r_2^{\bar{y}}\right)(\langle x, y, 2| + \langle y, x, 3|),$$
$$\langle\eta_3^L| = A_3 \sum_{x,y} r_1^{\bar{x}}\left(r_1^{\bar{y}} - r_2^{\bar{y}}\right)(\langle x, y, 2| - \langle y, x, 3|),$$
$$\langle\eta_4^L| = A_4 \sum_{x,y} r_1^{\bar{x}+\bar{y}}\langle x, y, 4|, \tag{5}$$

where $\bar{x} = N + 1 - x$, $\bar{y} = N + 1 - y$. It can be directly verified that $\langle\eta_m^L|\eta_n^R\rangle = 0$ for $m \neq n$ as required. Normalization constants $A_n \sim r_2^{-2N}$ so that $\langle\eta_n^L|\eta_n^R\rangle = 1$. The normalization constants are huge simply because left and right states are both well localized and spatially far away.

Now we are ready to calculate the driven response of the Hamiltonian, or equivalently, the Green's function of the system near zero energy. The benefit of finding the Jordan normal decomposition is that in order to solve the driven equation $(E - H)\psi = \xi$, we instead need to solve a much simpler equation $(E - J)\psi' = \xi'$, where $\psi' = P^{-1}\psi$, $\xi' = P^{-1}\xi$, and $(E - J)^{-1}$ is easy to compute. To understand the behavior of H near $E = 0$, we only need to work in the above mentioned four-dimensional subspace because only the vectors in this subspace can diverge as $1/E$ or faster. Therefore, below we appropriate the notations ξ' and ψ' to just represent the four-dimensional vectors. As mentioned, $(E - J_0)^{-1}$ is easy to compute:

$$(E - J_0)^{-1} = \begin{pmatrix} 1/E & 2\kappa/E^2 & 0 & 0 \\ 0 & 1/E & 0 & 0 \\ 0 & 0 & 1/E & \kappa/E^2 \\ 0 & 0 & 0 & 1/E \end{pmatrix}. \tag{6}$$

Because of the form of η_n^L, placing a source on sublattice 1 gives $\xi' \propto (1, 0, 0, 0)^T$. By calculating $\psi' = (E - J_0)^{-1}\xi'$ we see that the monosublattice state is excited. Likewise, placing a source on sublattice 4 induces $\xi' \propto (0, 0, 0, 1)^T$, so the multisublattice state is excited. Note that placing a source on either sublattice 2 or 3 induces $\xi' \propto (0, 1, \pm 1, 0)^T$, but the monosublattice state still dominates due to its faster divergence rate $1/E^2$. This is clearly observed in Fig. 4, where the response to the sources placed on sublattices 2 and 4 (middle and left figures) is stronger than that to the source placed on sublattice 1 (left figure). Remarkably, placing the source as far away as possible from the corner states leads to stronger excitation of the latter because the localization of the η_n^L at the bottom-right corner maximizes the overlap. The huge amplitude of the response ψ (see Fig. 4) is mainly due to the exponentially large normalization constant A_n. Such nonlocal response in the intermediate regime presents a remarkable opportunity for *unidirectional amplification* of corner states. Specifically, placing a source at the bottom-right corner will lead to huge response at the top-left corner, but a source at the top-left corner will only lead to weak response throughout

the system in comparison [29]. Compared to the response of an isolated site to the same source, whose amplitude would simply be $|1/E|$, the amplitude of the response of an array is amplified by roughly $|A_n|$ [Fig. 4(a)] or $|A_n\kappa/E|$ [Figs. 4(b) and 4(c)]. Such behavior is absent in the near-Hermitian regime since there the left and right eigenstates of a corner state are localized at the same corner [29]. Such unidirectional amplification can also be realized for the non-Hermitian SSH model [33] because the latter possesses a similarly defined intermediate regime. An important advantage of the non-Hermitian QI is that we can selectively excite two distinct corner states, whereas only one boundary state is supported by a 1D chain in the intermediate regime of the non-Hermitian SSH model.

Conclusions. The importance of Jordan decomposition instead of eigendecomposition in non-Hermitian systems is manifested in a non-Hermitian quadrupole insulator with asymmetric intracell coupling strengths, where it is crucial in identifying all "good approximate eigenstates" at zero energy and explain the delicate and exotic response of the system to external drives. We identified a previously unknown "intermediate regime" in the parameter space, where two types of corner states coexist, the Hamiltonian matrix becomes defective at zero energy, and unidirectional amplification of corner states is possible. While our system is analytically solvable, the numerical Schur decomposition is applicable to general non-Hermitian systems.

Acknowledgments. This work was supported by the US Department of the Navy, Office of Naval Research (ONR) under Grant No. N00014-17-1-2161, by the National Science Foundation (NSF) under Grant No. DMR-1741788, and by the Cornell Center for Materials Research with funding from the NSF MRSEC program (DMR-1719875). M.J. was supported in part by Kwanjeong Educational Foundation.

[1] W. A. Benalcazar, T. Li, and T. L. Hughes, Phys. Rev. B **99**, 245151 (2019).
[2] C.-Y. Hou, C. Chamon, and C. Mudry, Phys. Rev. Lett. **98**, 186809 (2007).
[3] M. Serra-Garcia, V. Peri, R. Süsstrunk, O. R. Bilal, T. Larsen, L. G. Villanueva, and S. D. Huber, Nature (London) **555**, 342 (2018).
[4] C. W. Peterson, W. A. Benalcazar, T. L. Hughes, and G. Bahl, Nature (London) **555**, 346 (2018).
[5] S. Imhof, C. Berger, F. Bayer, J. Brehm, L. W. Molenkamp, T. Kiessling, F. Schindler, C. H. Lee, M. Greiter, T. Neupert *et al.*, Nat. Phys. **14**, 925 (2018).
[6] X. Ni, M. Weiner, A. Alù, and A. B. Khanikaev, Nat. Mater. **18**, 113 (2019).
[7] W. A. Benalcazar, B. A. Bernevig, and T. L. Hughes, Science **357**, 61 (2017).
[8] W. A. Benalcazar, B. A. Bernevig, and T. L. Hughes, Phys. Rev. B **96**, 245115 (2017).
[9] H. C. Baker, Phys. Rev. A **30**, 773 (1984).
[10] K. Lopata and N. Govind, J. Chem. Theory Comput. **9**, 4939 (2013).
[11] W. Heiss, J. Phys.: Math. Gen. **37**, 2455 (2004).
[12] M. V. Berry, Czechoslov. J. Phys. **54**, 1039 (2004).
[13] N. Moiseyev, *Non-Hermitian Quantum Mechanics* (Cambridge University Press, Cambridge, 2011).
[14] L. Feng, R. El-Ganainy, and L. Ge, Nat. Photonics **11**, 752 (2017).
[15] R. El-Ganainy, K. G. Makris, M. Khajavikhan, Z. H. Musslimani, S. Rotter, and D. N. Christodoulides, Nat. Phys. **14**, 11 (2018).
[16] G. H. Golub and C. F. Van Loan, *Matrix Computations*, 4th ed. (Johns Hopkins University Press, Baltimore, MD, 2013).
[17] T. E. Lee, Phys. Rev. Lett. **116**, 133903 (2016).
[18] C. M. Bender, Rep. Prog. Phys. **70**, 947 (2007).
[19] C. T. West, T. Kottos, and T. Prosen, Phys. Rev. Lett. **104**, 054102 (2010).
[20] C. M. Bender, M. Gianfreda, Ş. K. Özdemir, B. Peng, and L. Yang, Phys. Rev. A **88**, 062111 (2013).
[21] A. Mostafazadeh, J. Math. Phys. **43**, 205 (2002).
[22] H. Shen, B. Zhen, and L. Fu, Phys. Rev. Lett. **120**, 146402 (2018).
[23] S. Yao and Z. Wang, Phys. Rev. Lett. **121**, 086803 (2018).
[24] T. Liu, Y.-R. Zhang, Q. Ai, Z. Gong, K. Kawabata, M. Ueda, and F. Nori, Phys. Rev. Lett. **122**, 076801 (2019).
[25] J. A. Sobota, S. Yang, J. G. Analytis, Y. L. Chen, I. R. Fisher, P. S. Kirchmann, and Z.-X. Shen, Phys. Rev. Lett. **108**, 117403 (2012).
[26] M. Marsi, Phys. Status Solidi RRL **12**, 1800228 (2018).
[27] S. Lieu, Phys. Rev. B **97**, 045106 (2018).
[28] C. Yin, H. Jiang, L. Li, R. Lü, and S. Chen, Phys. Rev. A **97**, 052115 (2018).
[29] See Supplemental Material at http://link.aps.org/supplemental/10.1103/PhysRevB.103.L041102 for derivation of the bulk spectrum of an open-boundary non-Hermitian QI, verification that the corner states given in the Letter are indeed approximate eigenstates of the system, demonstration of excitation of corner states of non-Hermitian QI in the near-Hermitian regime and excitation of edge states in a non-Hermitian SSH model, as well as how the steady state is established in the intermediate regime.
[30] L. Li, M. Umer, and J. Gong, Phys. Rev. B **98**, 205422 (2018).
[31] X.-R. Wang, C.-X. Guo, and S.-P. Kou, Phys. Rev. B **101**, 121116(R) (2020).
[32] K. B. Datta, *Matrix and Linear Algebra Aided with Matlab* (PHI Learning, New Delhi, 2016).
[33] J. C. Budich and E. J. Bergholtz, Phys. Rev. Lett. **125**, 180403 (2020).